Normal force and displacement amplitude influences on silver-plated electrical contacts subjected to fretting wear: a basic friction energy contact compliance formulation

F. Pompanon, J. Laporte, S. Fouvry, O. Alquier

Normal force and displacement amplitude influences on silver-plated electrical contacts subjected to fretting wear: a basic friction energy – contact compliance formulation

F.Pompanon[1], J. Laporte[1], S. Fouvry[1*], O. Alquier[2]

[1]LTDS, CNRS UMR 5513, Ecole Centrale de Lyon,

36 av Guy de Collongue, 69134 Ecully Cedex,

France

[2] PSA Groupe,

Vélizy - Villacoublay,

France

*Corresponding author: siegfried.fouvry@ec-lyon.fr

Abstract—During the last decades, the use of connectors in electrical devices for automotive has significantly increased. This raise in the number of electrical and electronic devices on board has led to a growing number of breakdowns. Indeed, this connectors need to keep a low and stable electrical contact resistance (ECR) but due to engine vibrations, fretting wear damage occur. Characterized by small oscillatory motions, fretting induces wear and oxide debris layer (third body) decaying the electrical contact resistance. The aim of this work is to study the effects of two main factors which are the normal contact force and the displacement amplitude. In this study, a silver-plated contact (2µm of thickness) was investigated applying various loading parameters: $2\ N < P < 6\ N$ and $\pm\ 3\mu m < \delta^* < \pm\ 20\ \mu m$. Results show that the ECR endurance decreases when the displacement amplitude increases regardless of the normal force. However, a non-monotonic evolution is found regarding normal force effect. Indeed, for a given displacement amplitude, a rise of the normal force tends to increase the contact pressure but at the same time induces a reduction of the effective sliding amplitude due a larger tangential accommodation. Hence by coupling a friction energy density approach with a basic compliance description, the synergic effect of the normal force and the displacement amplitude is described and the ECR endurance predicted.

Keywords— Fretting wear, electrical contact resistance, silver coating, normal force, friction energy

1. Introduction

In automotive applications, the use of connectors in electrical devices has significantly increased the last decades. These connectors must provide low and stable electrical contact resistance (ECR). However, due to their working environment (car engine), they are subjected to vibrations which induce fretting micro-displacements in the electrical contact.

Since the first studies realized by Antler [1], [2], the decay of electrical contact induced by fretting has been extensively investigated [3-12]. The best solution to reduce damage is to apply noble coatings such as gold and silver layers.

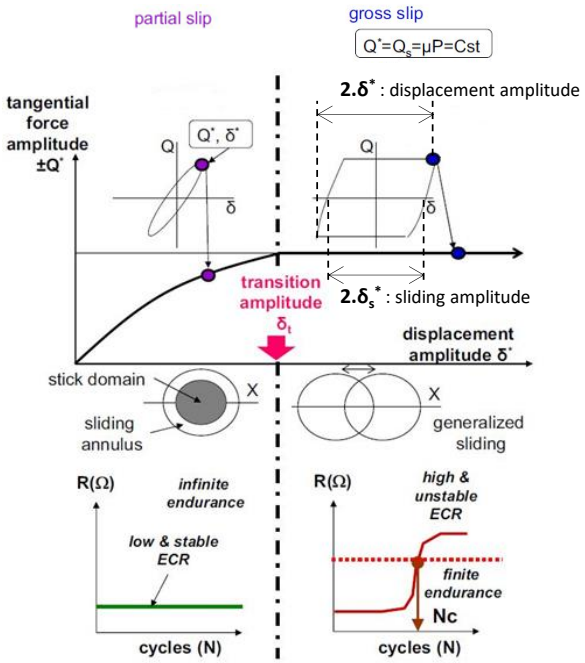

Fig. 1 : illustration of the influence of the sliding regime on the performance of electrical connectors: identification of finite and infinite behaviors

Various investigations, led by Kassman-Rudolphi and Jacobson [13], [14], Hannel et al. [15] and Laporte et al. [16] underline the critical influence of sliding regimes on electrical connector performances, as illustrated in Figure 1. Hence, as long as partial slip fretting conditions are maintained, an inner metal/metal stick zone operates, promoting stable and low ECR and infinite electrical endurance. In contrast, above a threshold displacement amplitude (δ_t^*), a gross slip condition operates, activating a wear process and the formation of low-conduction oxide debris which increase the ECR and lead to finite electrical endurance Nc (i.e. Nc = number of fretting cycles needed to reach a rising of the ECR above ΔR_{th}=4 mΩ). Hence it was shown a monotonic decrease of the electrical endurance, Nc, with the increase of

the fretting displacement amplitude (δ^*). However below the threshold displacement amplitude (δ_t^*), when the partial slip condition is stabilized, an infinite endurance is achieved. Such evolution was formalized using a power law description by Fouvry et al. [17] so that:

$$Nc = \frac{Nc_1}{(\delta^* - \delta_t)^n} \quad (1)$$

with Nc_1 = Nc (when $\delta^* - \delta_t$ = 1µm) and n the positive value of the ln(Nc) - ln($\delta^* - \delta_t$) decreasing slope.

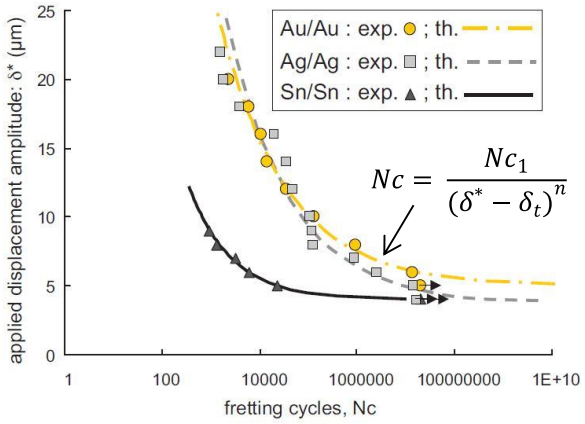

Fig. 2 : Comparison of endurance between experiments (exp.) and theoretical predictions provided by the power law (th.) (Eq. 1) for various materials [17]

Note that this very simple formulation can be applied whatever the studied material (Fig.2). The performance of the coating is calibrated by specific Nc_1, δ_t and n variables.

Simultaneously, numerous investigations were performed to correlate the surface degradation with the ECR evolution [12], [16], [17]. It was concluded that for noble coatings, the ECR decay is induced by the progressive elimination of the top silver or gold coating. It was demonstrated that the ECR failure (Nc) is reached when the atomic concentration of noble silver or gold element remaining in the debris layer within the interface becomes lower than 5% (Fig. 3):

Nc when $[Ag] < [Ag]_{th} \approx 5$ At%

where Nc is the ECR endurance related to the electrical failure when $\Delta R > \Delta R_{th=}4$ mΩ.

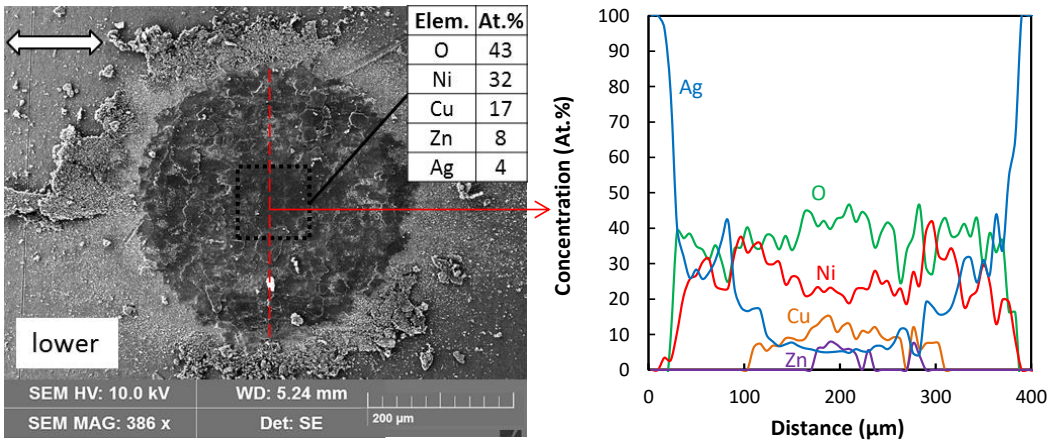

Fig. 3 : SEM observation and EDX analyses of a fretting scar (bottom specimen) at the electrical failure (Ag/Ag, f=30Hz, P=3N, T= 25°C, RH=10%,δ_0=9µm)

If the effect of the contact displacement and the surface degradation mechanism are now well described, the influence of the normal force load regarding ECR endurance is, in contrast, less clear.

Numerous investigations confirm that the wear rate is indirectly controlled by the friction work dissipated in the interface. The friction work is proportional to the sliding amplitude (δ_s^*) and the normal load (P). Hence assuming δ_s^* constant, an increase of the normal force promotes an increase of the friction work and therefore a reduction of the ECR endurance [16].

However it must be considered that in the actual situation of an industrial connector, it is not the sliding amplitude which is imposed but the displacement amplitude (δ^*) (Fig. 1). Taking into consideration this aspect, an increase of the normal force and therefore of the tangential amplitude promotes a rising of the tangential deformation of the test assembly. Hence for a given displacement amplitude, this induces a proportional reduction of the effective sliding amplitude operating inside the fretted interface. This reduction of the contact sliding decreases the sliding contribution regarding the friction work dissipated in the interface. For some conditions, this can balance the direct effect of the normal force so that the friction energy decreases and consequently the ECR endurance increases.

The aim of this paper is to clarify this aspect by developing an experimental investigation on silver plated (2µm) crossed-cylinder and by introducing a simple formulation based on the friction density approach to better formalize the effect of the normal force on the ECR endurance.

2. Experimental details

2.1 Materials

The samples used in the present study were crossed-cylinders with a homogenous Ag/Ag contact (i.e. similar upper and lower cylinders) (Fig. 4). The interface structure (Fig. 5) consisted in a 37 wt.% zinc (CuZn37) brass alloy substrate onto which a 2 µm electrolytic nickel interlayer was deposited in order to limit the copper diffusion. On this standard structure, 2 µm of pure silver was deposited using a dedicated electrolytic process.

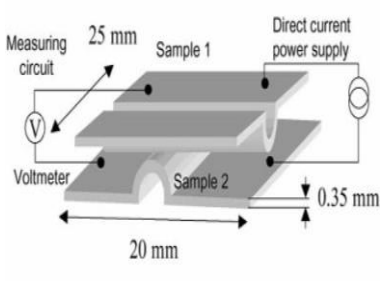

Fig. 4 : Sample configuration and electrical resistance measurement system

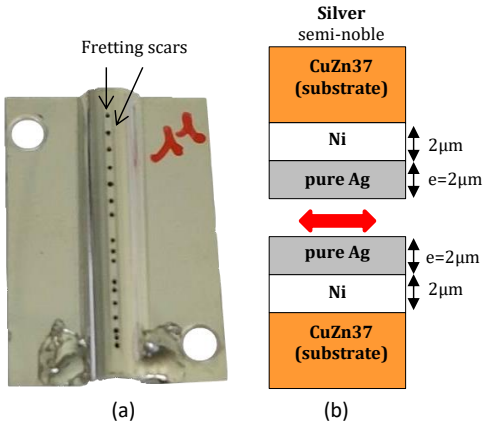

Fig. 5 : (a) Sample (b) Interface configuration of the samples

2.2 Contact Configuration and Electrical Resistance Measurement

The sample system used in this study consisted of two 90° crossed-cylinders with a 2.35mm cylinder radius (Fig. 4). According to the Hertzian theory, this contact configuration is equivalent to a sphere/plane contact with R=2.35 mm. During the test, the electrical contact resistance was measured using a 4-wire method. A current source applied I=5mA with 10V voltage compliance while a µvoltmeter system measured the contact voltage at a resolution of 0.01µV. This system makes it possible to measure the electrical resistance from 10^{-6} to 10^{3} Ω.

As previously mentioned, under gross slip condition, fretting wear damage reduces the ECR endurance. To quantify this aspect, the number of fretting cycles needed to reach the ΔR_{th}=4 mΩ ECR threshold inducing electrical failure is defined as Nc ECR endurance (Fig. 6).

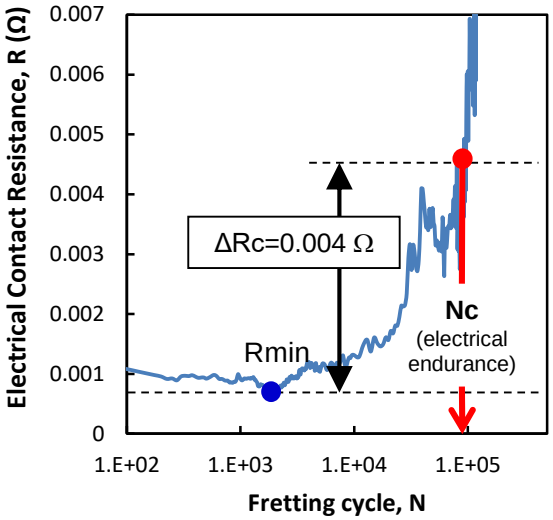

Fig. 6 : Criterion used to identify electrical endurance Nc (Ag/Ag, f=30Hz, P=3N, T= 25°C, RH=10%,δ_0=9µm)

Figure 6 represent the ECR evolution of the studied silver interface. It is interesting to underline the vertical rising of the ECR above Nc. Hence, it can be concluded that a variation of ΔR_{th} above the given threshold of 4 mΩ is not influencing the Nc endurance value.

2.3 Experimental Setup

Figure 7 shows a diagram of the machine used for this study. The fretting displacement (δ) was applied to the upper specimen using an electromagnetic shaker and measured using a high-resolution laser extensometer. The upper specimen holder was fixed to the shaker using flexure strips to guarantee the application of the normal force. The lower sample was fixed on the bottom specimen holder above which a piezoelectric load sensor allows the tangential force recording during the test. A dead mass was placed on the upper holder to assure the normal load.

In the present investigation, the temperature was controlled and fixed at 25 °C and the relative humidity maintained at 10%. Fretting tests were performed at a 30Hz frequency.

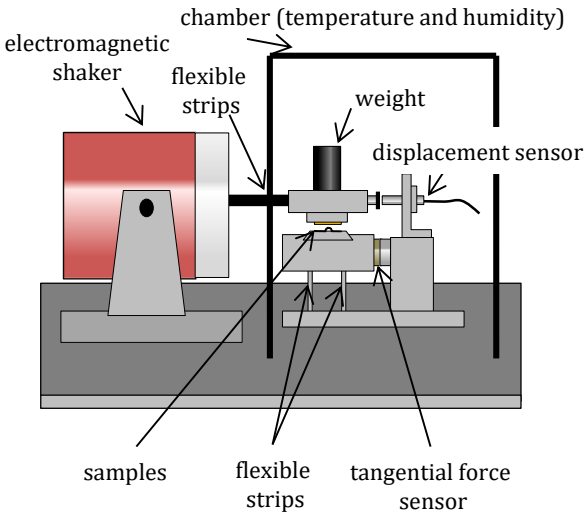

Fig. 7 : Diagram of the experimental set-up used in the study

2.4 Fretting loop analysis

As previously mentioned, a key aspect to investigate fretting wear is the plotting of the so-called "fretting loop" related to the evolution of the tangential force versus the applied displacement (Fig. 8).

The analysis of the fretting loop allows the determination of the tangential force amplitude (Q^*) and displacement amplitude (δ^*). However, the estimation of the real displacement in the contact is very difficult. Indeed, the displacement amplitude (δ^*) is measured outside the interface and includes the sliding amplitude (δ_s^*) but also the global tangential accommodation (δ_T^*) (i.e. apparatus and contact). This later can be assumed elastic which implies:

$$\delta^* = \delta_s^* + \delta_T^* = \delta_s^* + C_T \times Q^* \quad (2)$$

where C_T is the global elastic compliance (apparatus & contact) and Q^* the resulting tangential force amplitude.

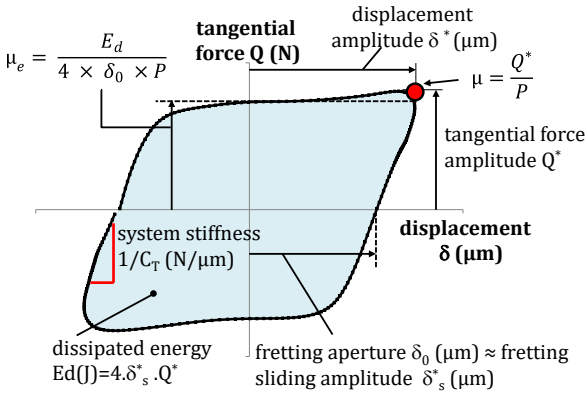

Fig. 8 : Analysis of the fretting cycle (gross slip condition) and definition of characteristic fretting parameters: δ* - displacement amplitude [µm], δ^*_s – sliding amplitude [µm], δ_0 – fretting cycle aperture [µm], Q tangential force [N].

The friction energy dissipated during a fretting cycle, E_d (J), was determined by integrating the δ - Q loop (i.e. area of the fretting cycle).

The friction coefficient, µ, is defined by:

$$\mu = \frac{Q^*}{P} \tag{3}$$

Finally, an averaged description of the friction behavior during the fretting cycle can be achieved using an "energy friction coefficient" [18]:

$$\mu_e = \frac{E_d}{4 \times \delta_0 \times P} \tag{4}$$

3. Results

3.1 Experimental analysis and analytical approximation of the partial slip/ gross slip transition.

As mentioned in introduction, as long as the contact is running under partial slip condition, the ECR endurance is infinite (regarding fretting wear process). Hence there is a key interest to express the displacement amplitude δ_t^* marking the transition between the partial slip (P.S) and the gross slip (G.S).

The studied crossed-cylinder interface is nearly equivalent to a sphere/plane configuration (with a similar sphere radius). Hence in first approximation, neglecting the presence of coating, the Hertzien and Mindlin formalisms are considered to describe the studied interface.

The determination of the sliding condition from the fretting cycle expertise is quite qualitative. To address a more quantitative approach, the energy sliding criteria A computed from the fretting cycle is considered so that [18] :

$$A = \frac{E_d}{E_t} = \frac{E_d}{4 \times \delta^* \times Q^*} \tag{5}$$

with E_t the corresponding friction energy obtained for a contact displaying an infinite stiffness.

For a sphere/plane contact it was shown that the P.S/G.S transition is related to a threshold value A_t=0.2 (i.e. when A > A_t=0.2 the contact is running under gross slip).

To experimentally established the P.S/G.S a variable displacement amplitude method (VDA) introduced by Voisin et al. [19] is applied. This method consists in increasing progressively the displacement amplitude and plotting the evolution of $\mu = Q^* / P$ and the energy ratio A. Hence the transition amplitude δ_t^* can be established from a single test.

Figure 9 displays an example of the method for a given normal force (P=2N). The displacement amplitude is progressively increased in small increments ($\Delta\delta^* = 0.5\mu m$). Each displacement amplitude is maintained for a sufficient time (ΔN = 15,000 cycles), so that the dynamic conditions in the contact are stabilized. The gradual increase of displacement allows the estimation of δ_t^* when the A ratio overpasses the A_t=0.2 threshold. For the studied test it was established around $\delta_t^* = \pm 2.5\ \mu m$. It is interesting to note that the P.S/G.S transition also corresponds to a friction coefficient discontinuity characterizing the interface shift from static friction to dynamical sliding.

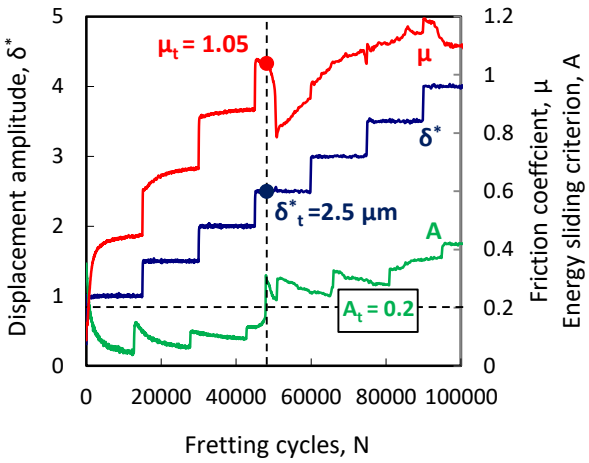

Fig. 9 : Variable displacement amplitude (VDA) method (Ag/Ag, f=30Hz, P=2N)

This methodology was applied for various normal forces (P = [2; 3; 4; 5; 6]) and the corresponding transition amplitudes are compiled in table 1 while the corresponding sliding condition fretting map (i.e. P - δ_t^*) is plotted in Figure 10.

P (N)	δ_t^* (± µm) (measured using VDA)	$\delta_{t,\,Mindlin}^*$ (± µm) (computed)	$\delta_{t,A}^* = \delta_t^* - \delta_{t,\,Mindlin}^*$ (± µm)
2	2.5	0.78	1.72
3	4	1.02	2.98
4	5.5	1.24	4.26
5	6.5	1.44	5.06
6	7.5	1.62	5.88

Table 1 : Transition amplitude, δ_t^* for various normal forces, obtained from VDA tests ($\delta_{t,\,exp}^*$) and the Mindlin formalism ($\delta_{t,\,Mindlin}^*$)

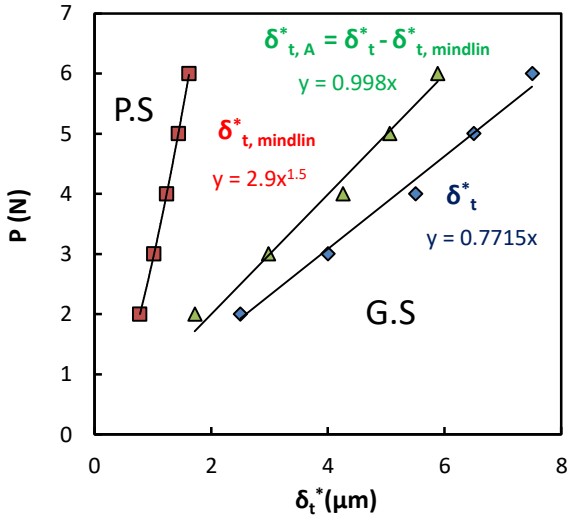

Fig. 10 : Evolution of the transition amplitude, δ_t^*, versus the normal force, obtained from VDA tests

The experimental δ_t^* P.S/G.S boundary is characterized by a quasi linear evolution passing through the origin.

As previously mentioned, a significantly part of the tangential displacement is accommodated by the apparatus. Hence the measured transition amplitude can be defined as the sum of the real contact displacement which can be approximate by the Mindlin theory [20, 21] ($\delta_{t,\,Mindlin}^*$) and the apparatus accommodation ($\delta_{t,A}^*$):

$$\delta_t^* = \delta_{t,\,Mindlin}^* + \delta_{t,A}^* \tag{6}$$

Assuming Hertzian hypothesis (elastic contact) [22] for semi-infinite solids the P.S/G.S transition can be expressed by the following relationship:

$$\delta_{t,Mindlin}^* = \frac{\mu \times P \times K_1}{a} \tag{7}$$

where

$$K_1 = \frac{3}{16} \times \left(\frac{2-\nu_1}{G_1} + \frac{2-\nu_2}{G_2}\right) \quad (8)$$

$$G = \frac{E}{2\times(1+\nu)} \quad (9)$$

$$a = \left(\frac{3\times P\times R^*}{4\times E^*}\right)^{\frac{1}{3}} \quad (10)$$

$$\frac{1}{E^*} = \frac{1-\nu_1^2}{E_1} + \frac{1-\nu_2^2}{E_2} \quad (11)$$

$$\frac{1}{R^*} = \frac{1}{R_1} + \frac{1}{R_2} \quad (12)$$

with a the Hertzian contact radius, E_1 and E_2 the elastic modulus of part 1 and 2, ν_1 and ν_2 their Poisson coefficient and R_1, R_2 the radius of the cross cylinders 1 and 2.

Note the formulation do not consider the coating.

For homogeneous contact (i.e. E = E1 = E2; $\nu = \nu_1 = \nu_2$ and $R = R_1 = R_2$) the former expression can be simplified and leads to:

$$\delta^*_{t,Mindlin} = \mu \times \frac{P^{2/3}}{R^{1/3}} \times K_M \quad (13)$$

with

$$K_M = \frac{3^{2/3}}{2^{5/3}\times E^{2/3}} \times \frac{(2-\nu)\times(1+\nu)}{(1-\nu^2)^{1/3}} \quad (14)$$

Assuming a friction coefficient $\mu = 1.05$, neglecting the presence of coatings and considering the elastic properties of the CuZn37 brass (E = 117 GPa and $\nu = 0.34$), the $\delta^*_{t,Mindlin}$ are computed and compiled in Table 1. Figure 10 plots the evolution of $\delta^*_{t,Mindlin}$ versus P. As expected from equation (13), a power law function is obtained so that:

$$P_t \propto {\delta^*_{t,Mindlin}}^{3/2} \quad (15)$$

Note that with Mindlin theory, the P.S/G.S transition is proportional to μ, $P^{2/3}$ and $R^{-1/3}$.

The Mindlin model provides very low values of the transition amplitude compared to the experimental results. This suggests that the test apparatus displays a very low tangential stiffness.

Then, the test apparatus $\delta_{t,A}^{*}$ can be extrapolated by subtracting the computed value of $\delta_{t,\,Mindlin}^{*}$ from δ_{t}^{*}. These values are compiled in Table 1 and plotted in Figure 10. A linear evolution passing through the origin is observed which confirms the idea that the test apparatus accommodation can be expressed as a linear expression with the normal load including the friction coefficient so that:

$$\delta_{t,A}^{*} = C_A \times Q_t^{*} = C_A \times \mu \times P \quad (16)$$

with C_A the apparatus compliance which was estimated around C_A = 0.95 µm/N for the studied test.

Finally the P.S/G.S transition can be approximated by the following simple expression:

$$\delta_{t}^{*} = \delta_{t,\,Mindlin}^{*} + \delta_{t,A}^{*} = \mu \times \left(K_M \times \frac{P^{2/3}}{R^{1/3}} + C_A \times P\right) \quad (17)$$

An interesting conclusion of this approximation is the fact that whatever the apparatus compliance, δ_t^{*} is proportional to the friction coefficient µ. Besides Figure 10 suggests a linear evolution of δ_t^{*} versus P with a slope established at 1/0.77. Assuming that the sliding amplitude is negligible at the PS/GS transition, Eq. 2 leads to:

$$\delta_{t}^{*} = C_T \times Q_t^{*} = C_T \times \mu \times P \quad (18)$$

where $C_T = \frac{1}{0.77\times\mu} = \frac{1}{0.77\times 1.05} = 1.22\ \mu m/N$

Coupling Eq. 17 and Eq. 18 it can be concluded that the global tangential compliance may be expressed by:

$$C_T = \frac{K_M}{(P\times R)^{1/3}} + C_A \quad (19)$$

Hence C_T depends on P to the power -1/3 but due to the dominating effect of the apparatus compliance (C_A) a constant value (C_T = 1.22 µm/N) is presently considered.

3.2 Endurance tests results

Once the P.S/G.S boundary established, fretting tests were performed under gross slip condition for various displacement amplitudes (δ^{*}) and various normal forces.

Figure 11 plots the evolution of the ECR endurance, Nc, versus the applied normal force, P, for various displacement amplitudes, δ^{*}. It is interesting to observe a non-monotonous evolution of the ECR endurances. First, Nc tends to decrease with the applied normal load, especially for displacement amplitude above 9 µm. This behavior suggests that the friction dissipation and the related surface wear are firstly increasing with the normal force. Then Nc remains quasi constant between P = 3N and P = 5 N whatever the displacement amplitude.

Finally, above P=5N, a sharp increase of Nc is observed for the smallest displacement amplitudes. This suggests that above a threshold normal load, the relative sliding is considerably reduced, inducing a sharp decrease of the wear rate.

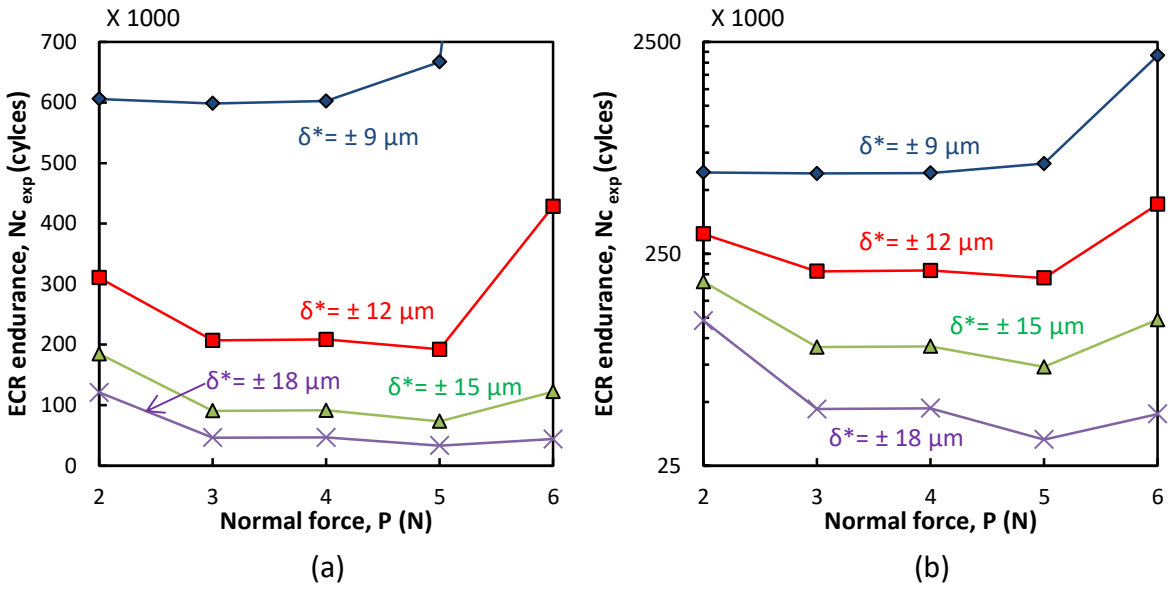

Fig. 11 : Evolution of Nc versus P for various displacement amplitudes (Ag/Ag, f=30Hz, T=25°C, RH=10%): (a) linear scale; (b) logarithmic scale

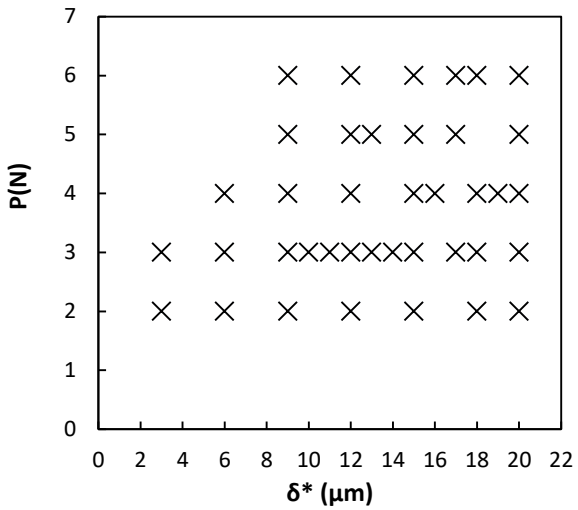

Fig. 12 : Mapping of the experimental tests performed

To complete this experimental investigations, an extensive mapping of the P - δ^* test conditions was adopted (3 µm < δ* < 20µm and 2N < P < 6 N) (Fig. 12). The obtained data were compiled to extract fretting mappings of the endurances, Nc, (Fig. 13 a) and the friction energy dissipated per cycle, E_d (Fig.13 b).

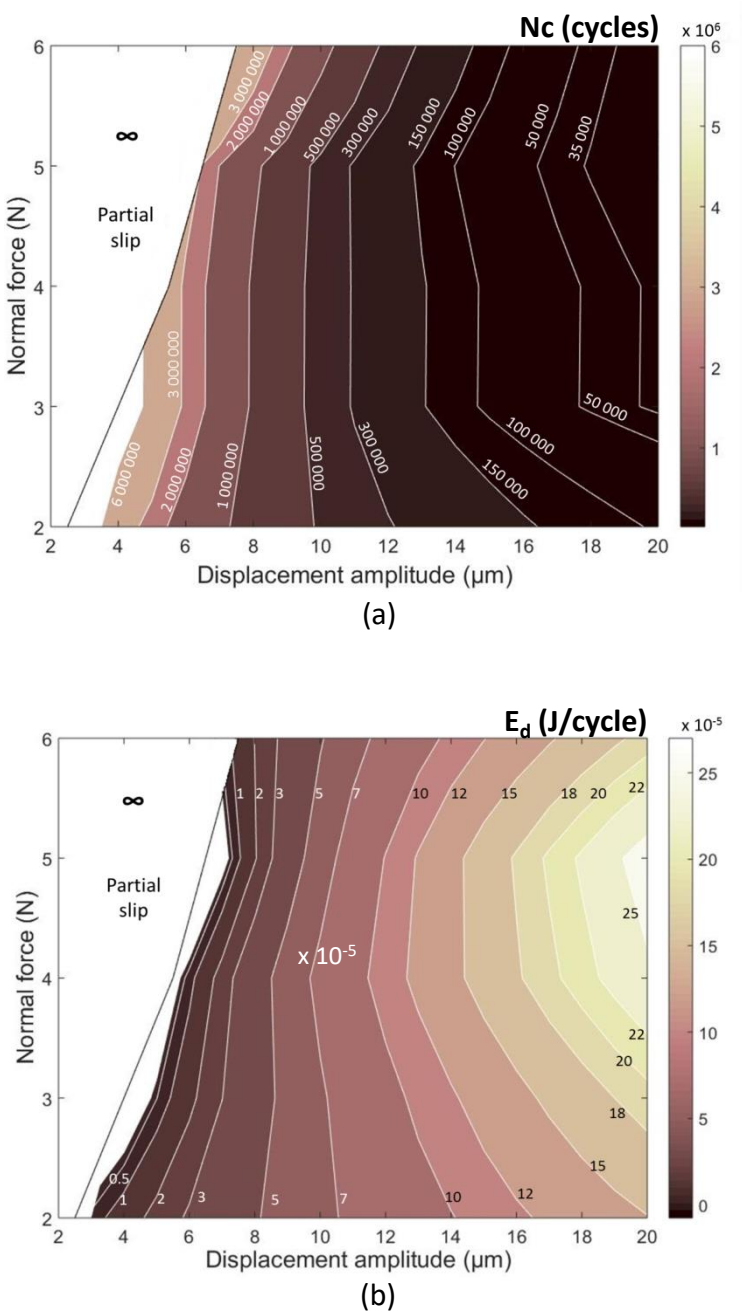

Fig. 13 : Experimental mapping of : (a) the ECR endurances, Nc (cycles); (b) the friction energy, E_d (J/cycle).

First, as mentioned in introduction (Fig. 2), for a given normal force, the Nc endurances display a sharp increase when the displacement amplitude decrease. When the displacement amplitude decrease below the threshold value δ_t^*, which depends on the normal force, an infinite endurance is achieved in the partial slip condition.

Then, as expected from the Nc endurances chart (Fig. 12), "U shape" iso-endurance curves can be observed (Fig.13 a). The same "U-shape" iso- friction energy can be observed (Fig. 13

b) with an opposite evolution. The higher the friction energy dissipated, the lower the Nc endurance confirming that the ECR endurance depends directly on the friction energy.

4. Modeling

4.1 Evolution of the friction energy, E_d

The evolution of the fretting loop with the normal force in gross slip condition is illustrated in Figure 14.

The first key aspect is the reduction of the sliding amplitude when the normal force increases. Assuming a constant displacement amplitude, δ^*, when a low normal force and thus a low tangential force is applied (Eq. 3), the tangential accommodation, δ_T^*, is rather small and most of the applied displacement is converted into sliding (Fig.14.1).

When the normal force as well as the tangential force increases, the tangential accommodation (i.e. contact, specimen and apparatus accommodation) is proportionally increased and consequently the effective sliding amplitude is reduced:

$$\delta_s^* = \delta^* - \delta_T^* = \delta^* - C_T \times Q^* \tag{20}$$

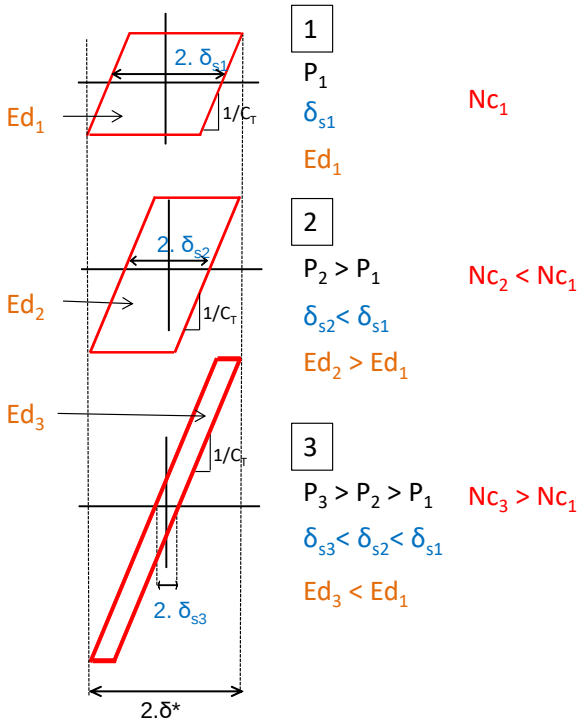

Fig. 14 : Evolution of the fretting loop with the normal force in gross slip condition

Simultaneously with the reduction of the sliding amplitude, the increase of the normal force leads to an increase of the tangential force (Q^*= μ.P) (the fretting loop becomes "taller"). As previously mentioned, the ECR endurance depends directly on the wear rate and consequently on the friction energy (i.e. area of the fretting loop).

Thus, the synergy between the reduction of the sliding amplitude and the increase of the tangential force cause a non-monotonic evolution of the friction energy when the normal force increases. First, the increase of the tangential force is preponderant, the friction energy increases (Fig. 14. 2) leading to a reduction of the endurance Nc. Then, the reduction of the sliding amplitude becomes major, thus the friction energy decreases (i.e. the area of the fretting loop reduces) leading to an increase of the endurance Nc (Fig. 14. 3).

Hence there is a key interest to express the evolution of the friction energy as a function of δ^* and P.

4.2 Formalization of the evolution of the friction energy, E_d

Assuming a trapezoidal description of the fretting loop, the friction energy (i.e. fretting loop area) may be approximated by:

$$E_d = 4 \times \delta_s^* \times \mu_e \times P \quad (21)$$

By combining the equations (4), (20) in (21) it leads to:

$$E_{d,th} = 4 \times \mu_e \times (P \times \delta^* - C_T \times \mu \times P^2) \quad (22)$$

With μ_e = 0.9, μ = 1.05 and C_T = 1.22 μm/N

Figure 15 plots the evolution of the theoretical friction energy (Eq. 22) in the normal load range [2N – 6N] for the studied displacement amplitudes used to compare the ECR endurances in Fig. 11.

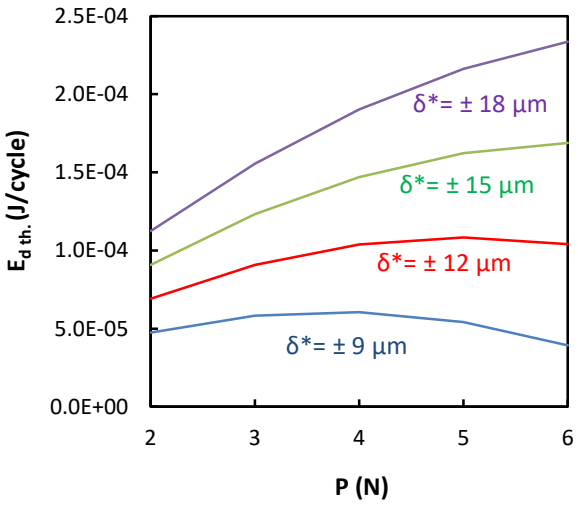

Fig.15 : Evolution of $E_{d\ th.}$ (Eq. 22) versus P for various displacement amplitudes (μ_e = 0.9, μ = 1.05, C = 1.22 µm/N)

As for the Nc analysis, non-monotonous evolutions are observed for the δ^* = ±9µm and δ^* = ±12µm. The maximum of friction energy are observed between P=4N and P=5N which corresponds to the lowest ECR endurances shown in Figure 11. The largest displacements (the δ^* = ±15µm and δ^* = ±18µm) promote a continuous increase of the friction energy which can be related to a lower increase of Nc for δ^* = ±15µm or a stabilization for δ^* = ±18µm (Fig. 12). Such a correlation between E_d and Nc confirms that Nc is function of the wear rate which itself depends of the friction work. Moreover, it justifies the non-monotonic evolutions of Nc observed in Figure 11 for δ^* < 18µm.

4.3 Formalization of the ECR endurance, Nc_{th}

Former investigations suggest that the ECR endurance may be expressed as a decreasing power law function of the mean friction energy density dissipated in the interface, φ [16]. This variable can be approximated using the following formulation:

$$\varphi = \frac{E_d}{A} \tag{23}$$

with Ed the averaged friction energy dissipated per fretting cycle during the test up to the Nc ECR failure:

$$E_d = \frac{\sum E_{d_{Nc}}}{Nc} \tag{24}$$

and A the final contact area measured at the electrical failure.

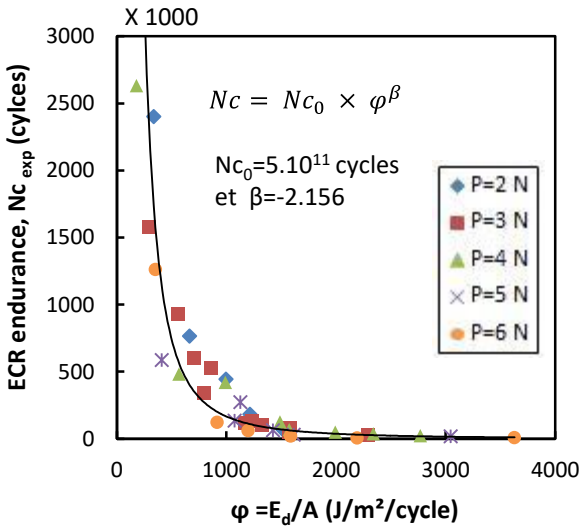

Fig. 16: Evolution of the ECR endurances (Nc) as a function of the friction energy density (φ) dissipated per cycle (Ag/Ag, f=30Hz, T=25°C, RH=10%, 2N < P < 6N, ±3µm < δ* < ±20µm)

Figure 16 plots the evolution of the Nc endurances obtained from the test matrix (Fig. 12) versus the corresponding friction energy density, φ.

All the points follow a single master curve which confirms the correlation between the ECR endurance and the friction energy density dissipated in the interface. A power law can be expressed so that:

$$Nc = Nc_0 \times \varphi^{\beta} \quad (25)$$

with Nc_0 the endurance when φ = 1 J/m²/cycle. For the studied interface Ag/Ag the coefficients $Nc_0 = 5.10^{11}$ cycles and β = 2.156 were found.

To predict Nc, the friction energy density, φ, need to be formalized and thus the evolution of the contact area, A, need to be studied.

Figure 17 plots the contact area, A, at the Nc failure versus the applied normal load P.

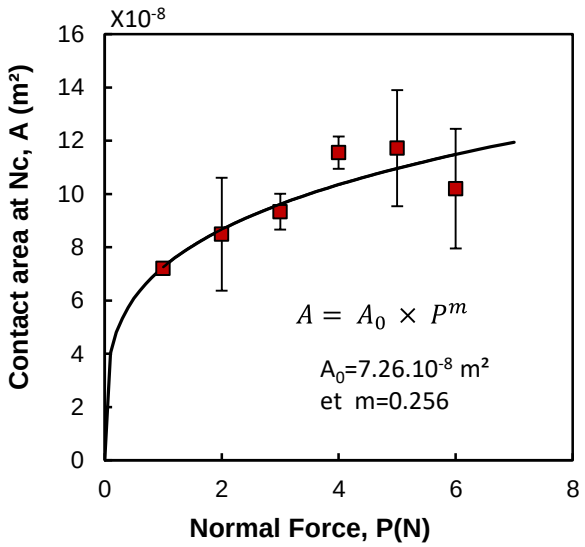

Fig. 17: Mean contact area at the ECR failure versus the normal force (Ag/Ag, f=30Hz, T=25°C, RH=10%, ±3µm < δ* < ±20µm)

As in previous studies [16], a power law function can be used to describe the asymptotic rising:

$$A = A_0 \times P^m \tag{26}$$

For the studied interface Ag/Ag the coefficients A=7.26.10^{-8} m² and m=0.256 were found.

Hence, the friction energy density can be approximated coupling Eq. (22), (23) and (26):

$$\varphi = \frac{4 \times \mu_e \, (P \times \delta^* - C_T \times \mu \times P^2)}{A_0 \times P^m} \tag{27}$$

$$\varphi = \frac{4 \times \mu_e}{A_0} \times P^{1-m} \times (\delta^* - C_T \times \mu \times P) \tag{28}$$

Finally, the predicted ECR endurance is extrapolated by coupling Eq.(25) and (27):

$$Nc_{th} = Nc_0 \times \left[\frac{4 \times \mu_e \times (P \times \delta^* - C_T \times \mu \times P^2)}{A_0 \times P^m}\right] \tag{29}$$

Note that two friction coefficients are considered in this formulation due to the rise of Q* during the sliding plateau (Fig. 8). For a constant friction condition (µ = µe), the previous expression is simplified accordingly.

5. Discussion:

Figure 18 compares the experimental ECR endurances with the theoretical ones extrapolated from Eq. 29.

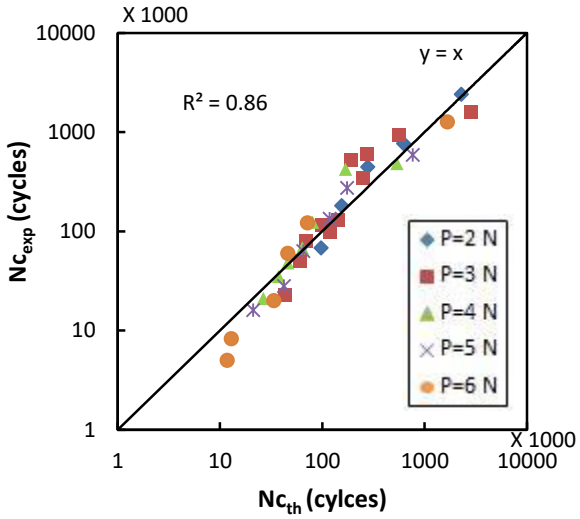

Fig. 18: Comparison between the experimental and the predicted (Eq. 29) ECR endurances.

A very good correlation is achieved which once again confirms the relevance of the friction energy density approach to predict the ECR endurance. An interesting result of this analysis is the introduction of an explicit formulation of the φ variable as a function of the applied displacement amplitude and the normal force taking into account the accommodation through the compliance parameter C_T.

Thus, using this basic formulation it is possible to extrapolate the φ – fretting map quantifying the dissipation as a function of the normal load and the displacement amplitude (Fig. 19 a) but also the corresponding predicted ECR endurances Nc (Fig. 19 b).

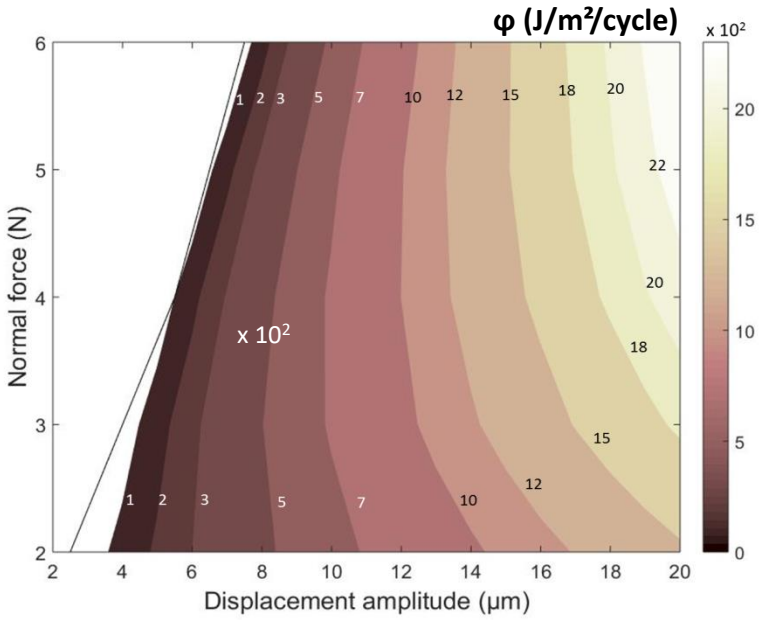

(a)

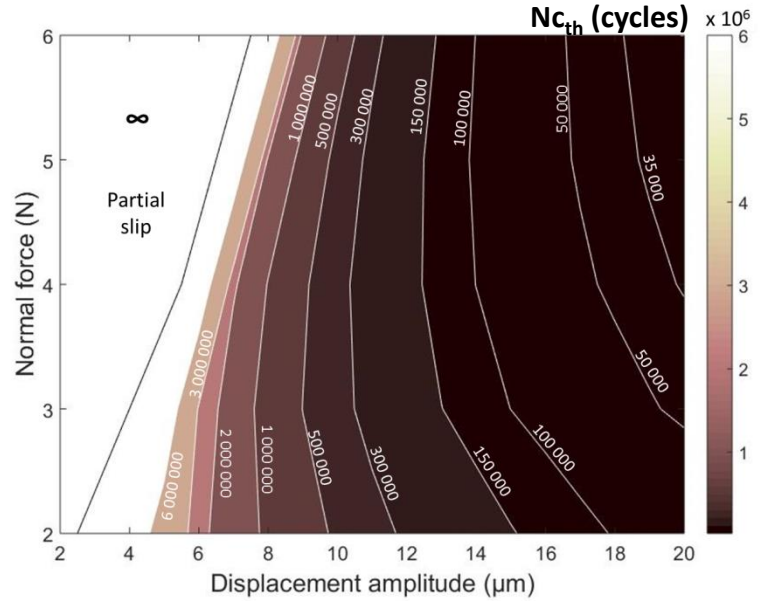

(b)

Fig. 19: Theoretical mapping of: (a) the friction energy density, φ_{th} (J/m²/cycle) (Eq.27); (b) the ECR endurances, Nc_{th} (cycles) (Eq.29).

A very good correlation is observed between the experimental (Fig. 13) and the predicted (Fig. 19) Nc – Fretting maps.

Similar positive slops are observed for the Nc iso-endurance curves close to the P.S/G.S transition (low displacement amplitudes, $\delta^* < 9\mu m$) which progressively take a "U shape" ($9\mu m < \delta^* < 16\ \mu m$) and finally become asymptotic decreasing curves for the higher displacement amplitudes above $\delta^* = 16\mu m$.

Thus, for a given displacement amplitude $\delta^* \leq 9\mu m$, the Nc endurances increase versus the normal load. Then, for $9\mu m < \delta^* < 16\ \mu m$, the Nc endurances display a "U shape" evolution with a minimum of endurance for P=4N and P= 5N. Finally for the higher displacement amplitudes, $\delta^* > 16\mu m$, the Nc endurances display an asymptotic decrease versus P. These three different behaviors are also well illustrated in Figure 20 which plots the evolution of the experimental and theoretical Nc endurances versus the normal force for various displacement amplitudes. Once again, the Nc fluctuations are well predicted.

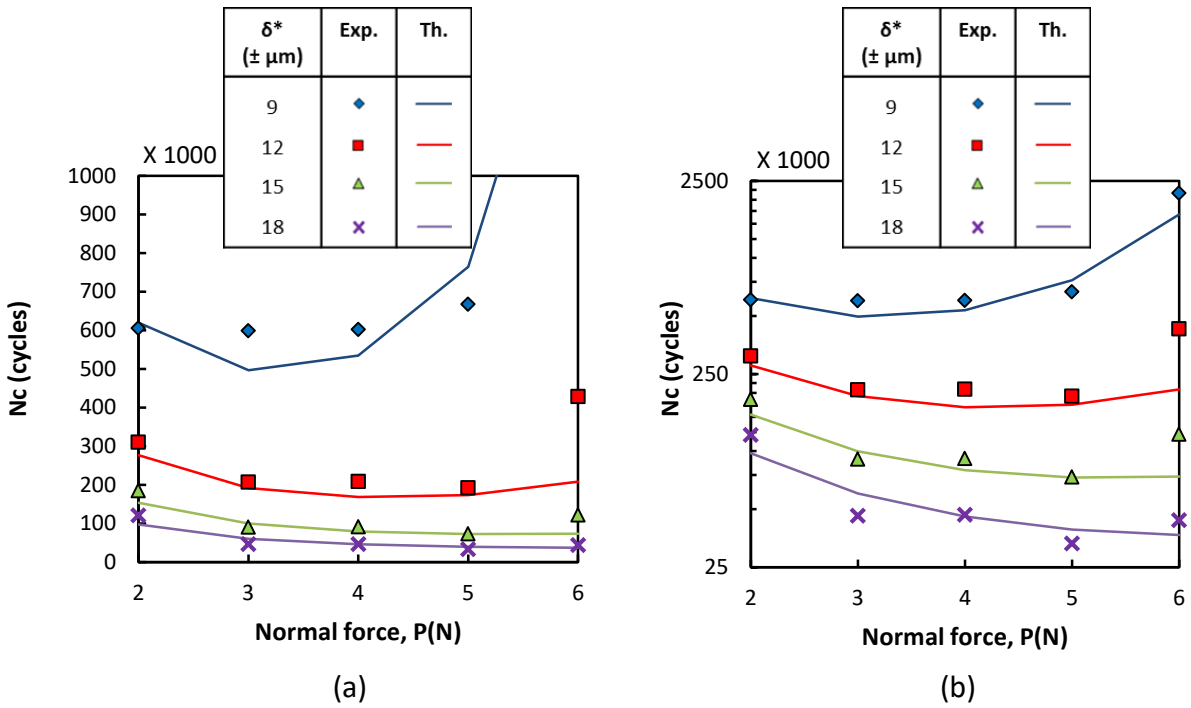

Fig. 20: Comparison between experimental and predicted Nc_{th} (Eq. 29) ECR endurances versus normal load for various displacement amplitudes with (a) a linear scale; (b) a logarithmic scale

Despite the simplicity of the formulation (Eq. 29) and the limited number of variables required to calibrate the model (i.e. C, µ, A_0, m and β) a rather good prediction of the Nc endurances is achieved.

Hence using a very simple formalism derived from a friction energy density analysis of fretting wear, we demonstrate that it is possible to predict the Nc ECR endurance as a function of the normal load and the displacement amplitude. This approach which was established for a Ag/Ag interface could be applied for other noble interface such as Au/Au contacts. Further investigations are however required to evaluate if such approach can be applied for non-noble materials like Sn coating where the Nc endurance is mainly driven by the Sn debris oxidation kinetic.

6. Conclusion:

The synergistic effects of the normal force and the displacement amplitude regarding the ECR endurance evolution of a silver plated contact were investigated. Both infinite endurance domain (Partial Slip) and finite endurance domain (Gross Slip) were characterized.

The P.S/G.S boundary (δ_t^*) was expressed taking into account the Mindlin formalism and the elastic accommodation of the test apparatus.

For the studied test conditions, most of the displacement is in fact accommodated by the test apparatus hence a linear approximation can be considered:

$\delta_t^* = C_T \times \mu \times P$ with $C_T = \frac{K_M}{(P \times R)^{1/3}} + C_A$

with C_T the global tangential compliance and K_M an elastic constant.

The experimental analysis suggest a quasi-constant value for C_T (i.e. 1.22 µm/N) which can be explained by the dominating effect of the apparatus compliance (C_A) and a low dependence versus P (i.e. -1/3 exponent).

Regarding the electrical response in finite endurance domain, fretting tests were performed under gross slip condition for various displacements and forces in order to extract fretting endurance map. As mentioned in previous works, for a given normal force, the Nc endurances exhibit a sharp decrease with the increase of the displacement. However, the evolution of Nc versus the normal force is less obvious and depends on the displacement amplitude condition. For the studied test conditions it was shown that:

- $\delta^* \leq 9\mu m$, Nc increases versus P.
- $9\mu m < \delta^* < 16\ \mu m$, Nc displays a "U shape" non-monotonic endurance evolution.
- $\delta^* > 16\mu m$, Nc displays an asymptotic decrease versus P.

The friction energy dissipated during the test was also extracted and compiled to generate de similar $E_d = f(P, \delta^*)$ map. These two fretting maps highlight the direct link between the endurance and the friction energy: the higher the friction dissipation, the lower Nc.

It was shown that the non-monotonic evolution of E_d versus the normal force P is induced by the reduction of the effective sliding amplitude due to the increase of the tangential accommodation. Using a friction wear model, such evolution was formalized and the ECR endurance in gross slip domain was expressed using a very simple expression so that:

If $\delta^* < \delta_t^*$: $Nc \rightarrow \infty$

If $\delta^* > \delta_t^*$: $Nc = Nc_0 \times \left[\frac{4 \times \mu_e \times (P \times \delta^* - C_T \times \mu \times P^2)}{A_0 \times P^m}\right]$

Despite the simplicity of the model, a very good correlation was observed with the experiments.

New aspects regarding the plasticity effect and the presence of debris layer may be considered in future developments. However, this research work suggests that a basic elastic-friction energy approach is suitable to calibrate the effect of the normal force and the displacement amplitude regarding the electrical performance of a silver plated interface.

7. References

[1] M. Antler, Electrical effects of fretting materials: a review*, Wear 106 (1985) 5–33.

[2] M. Antler and M. H. Drozdowicz, Fretting corrosion of gold-plated connector contacts, Wear 74 (1981) 27–50.

[3] R. D. Malucci, Characteristics of Films Developed in Fretting Experiments on Tin Plated Contacts, Proc. 45th IEEE HOLM (1999) 175–185.

[4] B. H. Chudnovsky, Degradation of Power Contacts in Industrial Atmosphere : Silver Corrosion and Whiskers, Proc. 48th IEEE Holm (2002) 140–150.

[5] M. Braunovic, Effect of intermetallic phases on the performance of tin-plated copper connections and conductors, Proc. 49th IEEE HOLM (2003) 124–131.

[6] N. Benjemaa and J. Swingler, Correlation between Wear and Electrical behaviour of contact interfaces during Fretting vibration, Proc. 23rd ICEC Conf. (2006) 215–219.

[7] S. Noël, D. Alamarguy, L. Baraton, and P. Laurat, Influence of Contact Interface Composition on the Electrical and Tribological Properties of Nickel Electrodeposits during Fretting Tests, Proc. 26th ICEC Conf. (2012).

[8] H. Essone-Obame, L. Cretinon, B. Cousin, N. Ben Jemaa, E. Carvou, and R. El Abdi, Investigation on friction coefficient evolution for thin-gold layer contacts, Proc. 26th ICEC Conf. (2012) 411–416.

[9] W. Ren, L. Cui, J. Chen, X. Ma, and X. Zhang, Fretting Behavior of Au Plated Copper Contacts Induced by High Frequency Vibration, Proc. 58th IEEE Holm (2012) 204–210.

[10] Y. Zhou, B. Yao, S. Ge, C. Hong, and J. Zhang, Failure Mechanism of Sliding Electrical Contacts with Various Plated Materials, Proc. 27th ICEC Conf. (2014) 108–113.

[11] H. J. Noh, J. W. Kim, S. M. Lee, and H. Jang, Effect of grain size on the electrical failure of copper contacts in fretting motion, Tribology International 111 (2017) 39–45

[12] F. Pompanon, S. Fouvry, and O. Alquier, Influence of humidity on the endurance of silver-plated electrical contacts subjected to fretting wear, Surface and Coatings Technology, 354 (2018) 246–256.

[13] A. Kassmann Rudolphi and S. Jacobson, Gross plastic fretting mechanical deterioration of silver coated electrical contacts, Wear 201 (1996) 244–254.

[14] Å. Kassman Rudolphi and S. Jacobson, Gross plastic fretting — examination of the gross weld regime, Wear 201 (1996) 255–264.

[15] S. Hannel, S. Fouvry, P. Kapsa, and L. Vincent, The fretting sliding transition as a criterion for electrical contact performance, Wear 249 (2001) 761–770

[16] J. Laporte, O. Perrinet, and S. Fouvry, Prediction of the electrical contact resistance endurance of silver-plated coatings subject to fretting wear, using a friction energy density approach, Wear 330-331 (2015) 170-181.

[17] S. Fouvry, P. Jedrzejczyk, and P. Chalandon, Introduction of an exponential formulation to quantify the electrical endurance of micro-contacts enduring fretting wear: Application to Sn, Ag and Au coatings, Wear 271 (2011) 1524–1534

[18] S.Fouvry, Ph Kapsa and L. Vincent, Quantification of fretting damage, Wear 200 (1996) 186-205

[19] J.M. Voisin et al., Analysis of a tube-grid oscillatory contact: methodology for the selection of superficial treatments, Wear 181–183 (1995) 826–832

[20] R. D. Mindlin, Compliance of elastic bodies in contact, J. Appl. Mech. 16 (1949) 259-268

[21] R. D. Mindlin and E. Deresiewicz, Elastic spheres in contact under varying oblique forces, J. Appl. Mech. 20 (1953) 327–344

[22] H. Hertz, Uber die beruhrung fester elasticher korper, J. Reine und Angew. Math. 92 (1882) 156–171